Navier-Stokes Flow in Cylindrical Elastic Tubes

Taha Sochi

University College London, Department of Physics & Astronomy, Gower Street, London, WC1E 6BT

Email: t.sochi@ucl.ac.uk.

Abstract

Analytical expressions correlating the volumetric flow rate to the inlet and outlet pressures are derived for the time-independent flow of Newtonian fluids in cylindrically-shaped elastic tubes using a one-dimensional Navier-Stokes flow model with two pressure-area constitutive relations. These expressions for elastic tubes are the equivalent of Poiseuille and Poiseuille-type expressions for rigid tubes which were previously derived for the flow of Newtonian and non-Newtonian fluids under various flow conditions. Formulae and procedures for identifying the pressure field and tube geometric profile are also presented. The results are validated by a finite element method implementation. Sensible trends in the analytical and numerical results are observed and documented.

Keywords: fluid mechanics; Navier-Stokes; one-dimensional flow; Newtonian fluids; cylindrical elastic tubes; finite element; time-independent; blood flow.

1   Introduction

Considerable amount of work has been done in the past on the flow in rigid tubes with different types of geometry for both Newtonian and non-Newtonian fluids using various derivation methods (see for example [1–8]). However, relatively little work has been done on the flow in elastic tubes especially on developing closed-form analytical relations. These relations are useful in many scientific, industrial and medical applications; an obvious example is the flow of blood in large vessels. Most of the reported work in the literature on the flow in elastic tubes is based on the use of numerical methods such as finite element (see for instance [9, 10]) mainly due to the fact that since the flow in networks of elastic tubes was the main focus of these studies numerical methods were more appropriate to use.

In the current paper, explicit analytical relations linking the volumetric flow rate to the pressure at the inlet and outlet are derived from a one-dimensional form

of the Navier-Stokes equations for cylindrically-shaped elastic tubes with constant cross sectional area using two pressure-area constitutive models. The flow rate formulae are validated by a finite element implementation based on a Galerkin method with Lagrange polynomial interpolation and Gauss quadrature integration schemes. Formulae implicitly defining the tube profile and pressure field at each point along the tube axis are also provided, demonstrated and validated. The results presented in this paper are especially useful in biological studies such as modeling blood flow in arteries and veins.

2 One-Dimensional Navier-Stokes Flow Model

The widely used one-dimensional Navier-Stokes model describing the flow of Newtonian fluids, which is mainly formulated to model the flow in elastic tubes, is given by the following mass and momentum conservation principles

$$\frac{\partial A}{\partial t} + \frac{\partial Q}{\partial z} = 0 \qquad t \geq 0, \ z \in [0, L] \qquad (1)$$

$$\frac{\partial Q}{\partial t} + \frac{\partial}{\partial z}\left(\frac{\alpha Q^2}{A}\right) + \frac{A}{\rho}\frac{\partial p}{\partial z} + \kappa\frac{Q}{A} = 0 \qquad t \geq 0, \ z \in [0, L] \qquad (2)$$

where A stands for the tube cross sectional area, t for time, Q for the volumetric flow rate, z for the space coordinate along the tube axis, L for the length of tube, α ($= \frac{\int u^2 dA}{A\overline{u}^2}$ with u and $\overline{u}$ being the fluid local and mean axial speed at the tube cross section respectively) for the axial momentum flux correction factor, ρ for the fluid mass density, p for the z-dependent pressure, and κ for the viscosity friction coefficient which is usually given by $\kappa = 2\pi\alpha\nu/(\alpha - 1)$ with ν being the fluid kinematic viscosity defined as the ratio of the dynamic viscosity μ to the mass density [9–12].

In using this model we assume a laminar, axi-symmetric, Newtonian, incompressible, fully-developed flow with insignificant gravitational forces and no-slip-at-wall boundary conditions [12, 13]. For our current purpose, we also assume a steady time-independent flow and hence we drop the time terms in the Navier-Stokes equations. In the following section, we use this one-dimensional Navier-Stokes formulation to derive Q-p relations for cylindrical elastic tubes using two pressure-area constitutive relations.

3 Deriving Q-p Relations

For time independent flow, the Navier-Stokes system given by Equations 1 and 2, becomes

$$\frac{\partial Q}{\partial z} = 0 \qquad z \in [0, L] \tag{3}$$

$$\frac{\partial}{\partial z}\left(\frac{\alpha Q^2}{A}\right) + \frac{A}{\rho}\frac{\partial p}{\partial z} + \kappa\frac{Q}{A} = 0 \qquad z \in [0, L] \tag{4}$$

The first of these equations states that Q as a function of z is constant. With regard to the second equation we have

$$\frac{A}{\rho}\frac{\partial p}{\partial z} = \frac{A}{\rho}\frac{\partial p}{\partial A}\frac{\partial A}{\partial z} = \frac{\partial}{\partial z}\int\frac{A}{\rho}\frac{\partial p}{\partial A}\frac{\partial A}{\partial z}\partial z = \frac{\partial}{\partial z}\int\frac{A}{\rho}\frac{\partial p}{\partial A}dA \tag{5}$$

Hence Equation 4 becomes

$$\frac{\partial}{\partial z}\left(\frac{\alpha Q^2}{A} + \int\frac{A}{\rho}\frac{\partial p}{\partial A}dA\right) + \kappa\frac{Q}{A} = 0 \qquad z \in [0, L] \tag{6}$$

3.1 First p-A Model

For this p-A model we assume a linear pressure-area constitutive relation and hence the pressure is proportional to the change in cross sectional area relative to the reference area, that is

$$p = \gamma\left(A - A_o\right) \tag{7}$$

where p is the actual pressure as opposed to the reference pressure to which the reference area is defined, γ is the proportionality coefficient which correlates to the tube stiffness, A is the tube cross sectional area at pressure p, and A_o is the reference area as identified by the reference pressure which, in this equation, is set to zero for convenience without affecting the generality of the results. From Equation 7, we get $\frac{\partial p}{\partial A} = \gamma$ and therefore

$$\int\frac{A}{\rho}\frac{\partial p}{\partial A}dA = \int\frac{A}{\rho}\gamma dA = \frac{\gamma A^2}{2\rho} \tag{8}$$

where the constant of integration is neglected because it will eventually vanish by the action of z partial derivative operator in Equation 6. Hence Equation 6 becomes

$$\frac{\partial}{\partial z}\left(\frac{\alpha Q^2}{A} + \frac{\gamma A^2}{2\rho}\right) + \kappa\frac{Q}{A} = 0 \tag{9}$$

that is

$$\frac{\partial}{\partial A}\left(\frac{\alpha Q^2}{A} + \frac{\gamma A^2}{2\rho}\right)\frac{\partial A}{\partial z} + \kappa\frac{Q}{A} = 0 \tag{10}$$

$$\left(-\frac{\alpha Q^2}{A^2} + \frac{\gamma A}{\rho}\right)\frac{\partial A}{\partial z} + \kappa\frac{Q}{A} = 0 \tag{11}$$

i.e.

$$\frac{\partial z}{\partial A} = \frac{\alpha Q}{\kappa A} - \frac{\gamma A^2}{\kappa\rho Q} \tag{12}$$

On integrating both sides of this equation with respect to A, which is always greater than zero, we get

$$z = \frac{\alpha Q}{\kappa}\ln A - \frac{\gamma}{3\kappa\rho Q}A^3 + C \tag{13}$$

where C is the constant of integration which can be obtained from one of the two boundary conditions, e.g. the inlet boundary condition where $A = A_{in}$ at $z = 0$ with A_{in} being the tube inlet area, that is

$$C = -\frac{\alpha Q}{\kappa}\ln A_{in} + \frac{\gamma}{3\kappa\rho Q}A_{in}^3 \tag{14}$$

Hence

$$z = \frac{\alpha Q}{\kappa}\ln\left(\frac{A}{A_{in}}\right) + \frac{\gamma}{3\kappa\rho Q}\left(A_{in}^3 - A^3\right) \tag{15}$$

Now, from this equation combined with the other boundary condition which defines the pressure at the outlet, that is $A = A_{ou}$ at $z = L$ where A_{ou} is the tube outlet area and L is the tube length, we obtain

$$L = \frac{\alpha Q}{\kappa}\ln\left(\frac{A_{ou}}{A_{in}}\right) + \frac{\gamma}{3\kappa\rho Q}\left(A_{in}^3 - A_{ou}^3\right) \tag{16}$$

This equation can be transformed to a quadratic polynomial in Q, i.e.

$$\frac{\alpha}{\kappa}\ln\left(\frac{A_{ou}}{A_{in}}\right)Q^2 - LQ + \frac{\gamma}{3\kappa\rho}\left(A_{in}^3 - A_{ou}^3\right) = 0 \tag{17}$$

with the following two roots

$$Q = \frac{L \pm \sqrt{L^2 - 4\frac{\alpha}{\kappa} \ln\left(A_{ou}/A_{in}\right) \frac{\gamma}{3\kappa\rho} \left(A_{in}^3 - A_{ou}^3\right)}}{2\frac{\alpha}{\kappa} \ln\left(A_{ou}/A_{in}\right)} \tag{18}$$

For $A_{in} > A_{ou}$, which can always be satisfied by proper labeling, the two roots are necessarily real. For a physically viable flow consistent in direction with the pressure gradient the negative sign should be taken to obtain a positive flow and hence

$$Q = \frac{L - \sqrt{L^2 - 4\frac{\alpha}{\kappa} \ln\left(A_{ou}/A_{in}\right) \frac{\gamma}{3\kappa\rho} \left(A_{in}^3 - A_{ou}^3\right)}}{2\frac{\alpha}{\kappa} \ln\left(A_{ou}/A_{in}\right)} \tag{19}$$

This is due to the fact that for $A_{in} > A_{ou}$ the denominator is negative and hence to obtain a positive flow rate the numerator should be negative as well, which is the case only if the negative sign is taken because the square root is always greater than L. This relation for elastic tubes is the equivalent of the Poiseuille equation for rigid tubes. However, for elastic tubes the flow rate is dependent not on the pressure difference but on the actual pressure at the inlet and outlet.

3.2 Second p-A Model

For the second pressure-area constitutive relation, the pressure is proportional to the radius change with a proportionality stiffness factor scaled by the reference area, that is

$$p = \frac{\beta}{A_o} \left(\sqrt{A} - \sqrt{A_o}\right) \tag{20}$$

where p is the pressure, β is the tube stiffness factor, A_o is the reference area at the reference pressure and A is the area at pressure p. The tube stiffness factor for the second p-A model is normally defined by the following relation

$$\beta = \frac{\sqrt{\pi} h_o E}{1 - \varsigma^2} \tag{21}$$

where h_o is the tube wall thickness at reference pressure, and E and ς are respectively the Young's elastic modulus and Poisson's ratio of the tube wall.

From the pressure-area constitutive relation of Equation 20 we obtain $\frac{\partial p}{\partial A} = \frac{\beta}{2A_o\sqrt{A}}$ and therefore

$$\int \frac{A}{\rho} \frac{\partial p}{\partial A} dA = \int \frac{A}{\rho} \frac{\beta}{2A_o\sqrt{A}} dA = \frac{\beta}{3\rho A_o} A^{3/2} \tag{22}$$

where the constant of integration is ignored as in the past. Hence Equation 6 becomes

$$\frac{\partial}{\partial z}\left(\frac{\alpha Q^2}{A} + \frac{\beta}{3\rho A_o}A^{3/2}\right) + \kappa\frac{Q}{A} = 0 \tag{23}$$

that is

$$\frac{\partial}{\partial A}\left(\frac{\alpha Q^2}{A} + \frac{\beta}{3\rho A_o}A^{3/2}\right)\frac{\partial A}{\partial z} + \kappa\frac{Q}{A} = 0 \tag{24}$$

i.e.

$$\left(-\frac{\alpha Q^2}{A^2} + \frac{\beta}{2\rho A_o}A^{1/2}\right)\frac{\partial A}{\partial z} + \kappa\frac{Q}{A} = 0 \tag{25}$$

Following similar steps to those outlined in the first model, we obtain

$$z = \frac{\alpha Q^2\ln\left(A/A_{in}\right) - \frac{\beta}{5\rho A_o}\left(A^{5/2} - A_{in}^{5/2}\right)}{\kappa Q} \tag{26}$$

From the last equation associated with the second boundary condition at the outlet, i.e. $A = A_{ou}$ at $z = L$, we obtain the following expression for the volumetric flow rate

$$Q = \frac{-\kappa L \pm \sqrt{\kappa^2 L^2 - 4\alpha\ln\left(A_{in}/A_{ou}\right)\frac{\beta}{5\rho A_o}\left(A_{ou}^{5/2} - A_{in}^{5/2}\right)}}{2\alpha\ln\left(A_{in}/A_{ou}\right)} \tag{27}$$

Both these solutions are necessarily real for $A_{in} > A_{ou}$ which can always be satisfied for normal flow conditions by proper labeling. For a flow which is physically-consistent in direction with the pressure gradient, the root with the plus sign should be selected, i.e.

$$Q = \frac{-\kappa L + \sqrt{\kappa^2 L^2 - 4\alpha\ln\left(A_{in}/A_{ou}\right)\frac{\beta}{5\rho A_o}\left(A_{ou}^{5/2} - A_{in}^{5/2}\right)}}{2\alpha\ln\left(A_{in}/A_{ou}\right)} \tag{28}$$

This, in essence, is a relation between flow rate and pressure drop, similar to the Poiseuille law for rigid tubes, although for elastic tubes the flow rate, as given by Equation 28, does not depend on the pressure difference, as for rigid tubes, but on the actual inlet and outlet pressure as defined by the inlet and outlet area respectively.

4 Finite Element Formulation

The flow formulae derived in the previous section can be validated by the finite element method using the weak formulation. This formulation is outlined for the first and second p-A models in the following two subsections. More details about the finite element technicalities and the solution scheme using Newton-Raphson iteration are given in [12].

4.1 First p-A Model

The Navier-Stokes system, given by Equations 1 and 2, can be cast in matrix form which is more appropriate for numerical manipulation and implementation as follow

$$\frac{\partial \mathbf{U}}{\partial t} + \frac{\partial \boldsymbol{F}}{\partial z} + \mathbf{B} = \mathbf{0} \tag{29}$$

where

$$\mathbf{U} = \begin{bmatrix} A \\ Q \end{bmatrix}, \qquad \boldsymbol{F} = \begin{bmatrix} Q \\ \frac{\alpha Q^2}{A} + \frac{\gamma A^2}{2\rho} \end{bmatrix}, \qquad \text{and} \qquad \mathbf{B} = \begin{bmatrix} 0 \\ \kappa \frac{Q}{A} \end{bmatrix} \tag{30}$$

On multiplying Equation 29 by weight functions and integrating over the solution domain, z, the following system is obtained

$$\int_{\Omega} \frac{\partial \mathbf{U}}{\partial t} \cdot \boldsymbol{\omega} dz + \int_{\Omega} \frac{\partial \mathbf{F}}{\partial z} \cdot \boldsymbol{\omega} dz + \int_{\Omega} \mathbf{B} \cdot \boldsymbol{\omega} dz = \mathbf{0} \tag{31}$$

where Ω is the solution domain, and $\boldsymbol{\omega}$ is a vector of arbitrary test functions. On integrating the second term of Equation 31 by parts, the following weak form of the preceding 1D flow system is obtained

$$\int_{\Omega} \frac{\partial \mathbf{U}}{\partial t} \cdot \boldsymbol{\omega} dz - \int_{\Omega} \mathbf{F} \cdot \frac{d\boldsymbol{\omega}}{dz} dz + \int_{\Omega} \mathbf{B} \cdot \boldsymbol{\omega} dz + [\mathbf{F} \cdot \boldsymbol{\omega}]_{\partial\Omega} = \mathbf{0} \tag{32}$$

where $\partial\Omega$ is the boundary of the solution domain. This weak formulation, coupled with suitable boundary conditions, can be used as a basis for finite element implementation in conjunction with an iterative scheme such as Newton-Raphson method. Following a solution scheme detailed in [12] and based on the method of characteristics [9, 10, 14–17], the eigenvalues $\lambda_{1,2}$ and left eigenvectors $\boldsymbol{L}_{1,2}$ of the $\mathbf{H}$ matrix, which are required for obtaining the compatibility conditions on the

boundaries, are found as follow

$$\det\left(\mathbf{H} - \lambda\mathbf{I}\right) = \det\left(\begin{bmatrix} -\lambda & 1 \\ -\frac{\alpha Q^2}{A^2} + \frac{\gamma A}{\rho} & \frac{2\alpha Q}{A} - \lambda \end{bmatrix}\right) = 0 \tag{33}$$

where $\mathbf{H}$ is the matrix of partial derivatives of $\mathbf{F}$ with respect to $\mathbf{U}$, that is

$$\mathbf{H} = \frac{\partial \mathbf{F}}{\partial \mathbf{U}} = \begin{bmatrix} 0 & 1 \\ -\frac{\alpha Q^2}{A^2} + \frac{\gamma A}{\rho} & \frac{2\alpha Q}{A} \end{bmatrix} \tag{34}$$

On solving Equation 33 the eigenvalues are obtained

$$\lambda_{1,2} = \frac{\alpha Q}{A} \pm \sqrt{\frac{Q^2}{A^2}\left(\alpha^2 - \alpha\right) + \frac{\gamma A}{\rho}} \tag{35}$$

which are necessarily real for $\alpha \geq 1$ as it is always the case, and hence the left eigenvectors are obtained

$$\boldsymbol{L}_{1,2} = \begin{bmatrix} -\alpha\frac{Q}{A} \pm \sqrt{\frac{Q^2}{A^2}\left(\alpha^2 - \alpha\right) + \frac{\gamma A}{\rho}} & 1 \end{bmatrix} \tag{36}$$

The compatibility conditions for the time-independent flow arising from projecting the differential equations in the direction of the outgoing characteristic variables at the inlet and outlet are then obtained from

$$\boldsymbol{L}_{1,2}\left(\mathbf{H}\frac{\partial \mathbf{U}}{\partial z} + \mathbf{B}\right) = 0 \tag{37}$$

that is

$$\begin{bmatrix} -\alpha\frac{Q}{A} \pm \sqrt{\frac{Q^2}{A^2}\left(\alpha^2 - \alpha\right) + \frac{\gamma A}{\rho}} & 1 \end{bmatrix} \begin{bmatrix} \frac{\partial Q}{\partial z} \\ \left(-\frac{\alpha Q^2}{A^2} + \frac{\gamma A}{\rho}\right)\frac{\partial A}{\partial z} + \frac{2\alpha Q}{A}\frac{\partial Q}{\partial z} + \kappa\frac{Q}{A} \end{bmatrix} = 0 \tag{38}$$

which can be simplified to

$$\left(-\alpha\frac{Q}{A} \pm \sqrt{\frac{Q^2}{A^2}\left(\alpha^2 - \alpha\right) + \frac{\gamma A}{\rho}}\right)\frac{\partial Q}{\partial z} + \left(-\frac{\alpha Q^2}{A^2} + \frac{\gamma A}{\rho}\right)\frac{\partial A}{\partial z} + \frac{2\alpha Q}{A}\frac{\partial Q}{\partial z} + \kappa\frac{Q}{A} = 0 \tag{39}$$

4.2 Second p-A Model

Following a similar procedure to that outlined in the previous subsection for the first p-A model, the finite element formulation leads to the following matrix structure, eigenvalues, left eigenvectors and time-independent compatibility conditions respectively

$$
\mathbf{U} = \begin{bmatrix} A \\ Q \end{bmatrix}, \qquad \mathbf{F} = \begin{bmatrix} Q \\ \frac{\alpha Q^2}{A} + \frac{\beta A^{3/2}}{3\rho A_o} \end{bmatrix} \qquad \text{and} \qquad \mathbf{B} = \begin{bmatrix} 0 \\ \kappa \frac{Q}{A} \end{bmatrix} \tag{40}
$$

$$
\lambda_{1,2} = \alpha \frac{Q}{A} \pm \sqrt{\frac{Q^2}{A^2}(\alpha^2 - \alpha) + \frac{\beta \sqrt{A}}{2\rho A_o}} \tag{41}
$$

$$
\boldsymbol{L}_{1,2} = \begin{bmatrix} -\alpha \frac{Q}{A} \pm \sqrt{\frac{Q^2}{A^2}(\alpha^2 - \alpha) + \frac{\beta \sqrt{A}}{2\rho A_o}} & 1 \end{bmatrix} \tag{42}
$$

and

$$
\left(-\alpha \frac{Q}{A} \pm \sqrt{\frac{Q^2}{A^2}(\alpha^2 - \alpha) + \frac{\beta \sqrt{A}}{2\rho A_o}} \right) \frac{\partial Q}{\partial z} + \left(-\alpha \frac{Q^2}{A^2} + \frac{\beta \sqrt{A}}{2\rho A_o} \right) \frac{\partial A}{\partial z} + \left(2\alpha \frac{\partial Q}{\partial z} + \kappa \right) \frac{Q}{A} = 0 \tag{43}
$$

5 Numerical Validation

To validate the derived flow formulae, the finite element formulation as outlined in the previous section was implemented for the two p-A models in a computer code using a Galerkin method with a Lagrange polynomial interpolation associated with a Gauss quadrature integration scheme. The comparison between the analytic and finite element solutions is outlined for some typical cases in the following two subsections.

5.1 First p-A Model

Extensive tests have been carried out to verify Equation 19; a sample of which is given in Table 1. Certain sensible trends can be observed in these results. For example, the diagonally-oriented entries from top-left to bottom-right direction in the table are of similar magnitude which is sensible since in this quasi-linear flow

regime obtained at relatively low pressures the flow is Poiseuille-like and hence it is almost proportional to the pressure difference (i.e. $P_{in} - P_{ou}$). This Poiseuille-like behavior disappears at high-pressure flow regimes as the flow rate becomes increasingly dependent on the actual pressures at the inlet and outlet rather than on the pressure difference. Another sensible trend is that the flow rate in these diagonally-oriented entries is increasing in the top-left to bottom-right direction due to the fact that although the pressure difference for these entries is the same, the lower entries have larger area at the inlet and outlet, due to the higher pressure at the tube entrance and exit, than the upper ones. This trend is more obvious at higher pressure regimes.

We also used Equation 15, which implicitly correlates A to z, to obtain the pressure field inside the tube and the tube profile by numerically solving for A for a given z. A sample of these results, with their finite element counterparts, is presented in Figures 1 and 2. These figures confirm the sensibility of the obtained analytical and numerical results.

Table 1: Sample results of the volumetric flow rate in m^3/s related to the elastic tube investigation for the first p-A model. The rows stand for the inlet pressure, P_{in}, and the columns for the outlet pressure, P_{ou}, in Pa. The parameters with which these results are obtained are: $\rho = 1060$ kg/m^3, $\mu = 0.0035$ Pa.s, $\alpha = 1.333$, $L = 1.0$ m, $r = 0.1$ m, and $\gamma = 5 \times 10^6$ Pa/m^2. In each P_{in} row the top and bottom entries are respectively the analytic solution, given by Equation 19, and the finite element solution which is obtained with a quadratic Lagrange polynomial interpolation.

| P_{in}	P_{ou} 0	100	200	300	400	500	600	700	800	900
100	0.286046									
	0.286046									
200	0.307977	0.286332								
	0.307977	0.286332								
300	0.315789	0.308278	0.286619							
	0.315789	0.308278	0.286619							
400	0.319850	0.316096	0.308579	0.286905						
	0.319850	0.316096	0.308579	0.286905						
500	0.322373	0.320158	0.316402	0.308881	0.287192					
	0.322373	0.320159	0.316402	0.308881	0.287192					
600	0.324118	0.322684	0.320467	0.316708	0.309182	0.287479				
	0.324119	0.322684	0.320467	0.316708	0.309182	0.287479				
700	0.325415	0.324430	0.322994	0.320776	0.317015	0.309484	0.287766			
	0.325415	0.324430	0.322994	0.320777	0.317015	0.309484	0.287766			
800	0.326430	0.325727	0.324741	0.323305	0.321086	0.317322	0.309785	0.288053		
	0.326430	0.325728	0.324742	0.323305	0.321086	0.317322	0.309785	0.288053		
900	0.327256	0.326743	0.326040	0.325053	0.323615	0.321395	0.317628	0.310087	0.288340	
	0.327257	0.326743	0.326040	0.325053	0.323616	0.321395	0.317628	0.310087	0.288340	
1000	0.327950	0.327569	0.327056	0.326352	0.325365	0.323926	0.321704	0.317935	0.310389	0.288627
	0.327951	0.327570	0.327056	0.326353	0.325365	0.323926	0.321704	0.317935	0.310389	0.288627
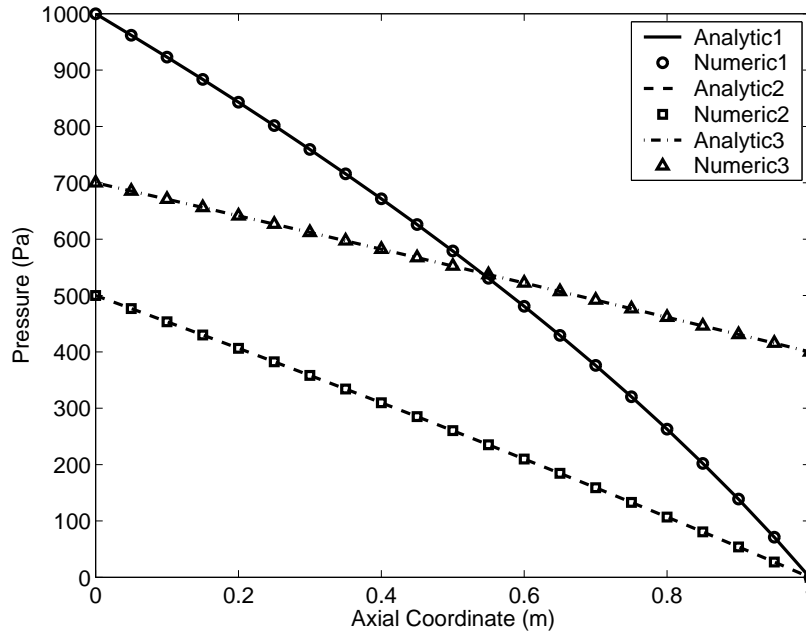
Figure 1: Pressure versus tube axial coordinate for three sample cases related to the first p-A model as obtained analytically from Equation 15 and numerically by a finite element method with a quadratic polynomial interpolation scheme as outlined in the previous section. The labels '1', '2' and '3' in these plots refer respectively to the cases where $P_{in} = 1000$ Pa and $P_{ou} = 0$ Pa, $P_{in} = 500$ Pa and $P_{ou} = 0$ Pa, and $P_{in} = 700$ Pa and $P_{ou} = 400$ Pa. The tube, fluid and flow parameters with which these results are obtained are: $\rho = 1060$ kg/m^3, $\mu = 0.0035$ Pa.s, $\alpha = 1.333$, $L = 1.0$ m, $r = 0.1$ m, and $\gamma = 5 \times 10^6$ Pa/m^2.
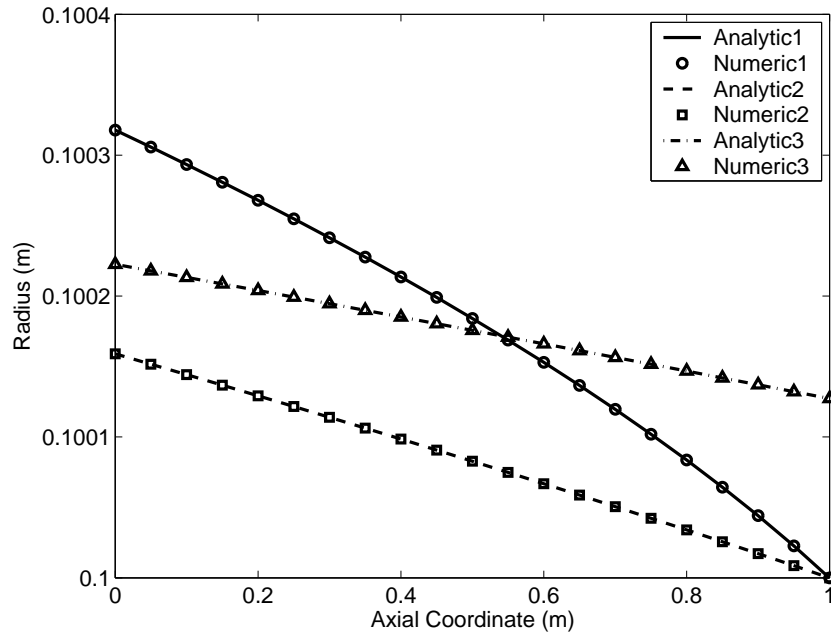

Figure 2: Radius versus tube axial coordinate for the three sample cases of Figure 1.

5.2 Second p-A Model

Extensive tests have been carried out to verify Equation 28; a sample of which is given in Table 2. Also, we used Equation 26 to obtain the pressure field inside the tube and the tube geometric profile, as outlined for the first p-A model. A sample of these results, with their finite element equivalents, is presented in Figures 3 and 4. Similar sensible trends to those observed in the first p-A model are detected.

Table 2: Sample results of the volumetric flow rate in m^3/s related to the elastic tube investigation for the second p-A model. The rows stand for the inlet pressure, P_{in}, and the columns for the outlet pressure, P_{ou}, in Pa. The parameters with which these results are obtained are: $\rho = 1060$ kg/m^3, $\mu = 0.0035$ Pa.s, $\alpha = 1.333$, $L = 1.0$ m, $r = 0.1$ m, and $\beta = 5 \times 10^4$ Pa.m. In each P_{in} row the top and bottom entries are respectively the analytic solution, given by Equation 28, and the finite element solution which is obtained with a quadratic Lagrange polynomial interpolation.

| P_{in}	P_{ou} 0	100	200	300	400	500	600	700	800	900
100	0.273135									
	0.273135									
200	0.292950	0.273397								
	0.292950	0.273397								
300	0.299986	0.293221	0.273659							
	0.299986	0.293221	0.273659							
400	0.303637	0.300259	0.293491	0.273922						
	0.303637	0.300259	0.293491	0.273922						
500	0.305904	0.303912	0.300532	0.293762	0.274184					
	0.305904	0.303912	0.300533	0.293762	0.274184					
600	0.307471	0.306180	0.304187	0.300806	0.294033	0.274447				
	0.307471	0.306180	0.304187	0.300806	0.294033	0.274447				
700	0.308634	0.307747	0.306455	0.304462	0.301080	0.294304	0.274710			
	0.308634	0.307747	0.306456	0.304462	0.301080	0.294304	0.274710			
800	0.309543	0.308910	0.308023	0.306731	0.304737	0.301353	0.294575	0.274973		
	0.309543	0.308910	0.308023	0.306731	0.304737	0.301353	0.294575	0.274973		
900	0.310283	0.309820	0.309187	0.308299	0.307007	0.305012	0.301627	0.294847	0.275236	
	0.310283	0.309820	0.309187	0.308300	0.307007	0.305012	0.301627	0.294847	0.275237	
1000	0.310903	0.310560	0.310097	0.309464	0.308576	0.307283	0.305287	0.301902	0.295118	0.275500
	0.310904	0.310561	0.310097	0.309464	0.308576	0.307283	0.305287	0.301902	0.295118	0.275500
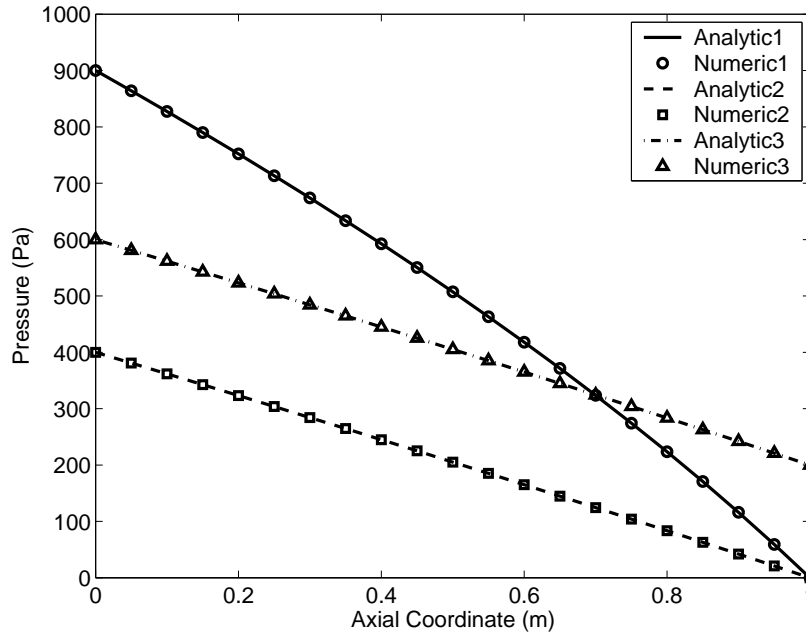
Figure 3: Pressure versus tube axial coordinate for three sample cases related to the second p-A model as obtained analytically from Equation 28 and numerically by a finite element method with a quadratic polynomial interpolation scheme as outlined in the previous section. The labels '1', '2' and '3' in these plots refer respectively to the cases where $P_{in} = 900$ Pa and $P_{ou} = 0$ Pa, $P_{in} = 400$ Pa and $P_{ou} = 0$ Pa, and $P_{in} = 600$ Pa and $P_{ou} = 200$ Pa. The tube, fluid and flow parameters with which these results are obtained are: $\rho = 1060$ kg/m^3, $\mu = 0.0035$ Pa.s, $\alpha = 1.333$, $L = 1.0$ m, $r = 0.1$ m, and $\beta = 5 \times 10^4$ Pa.m.
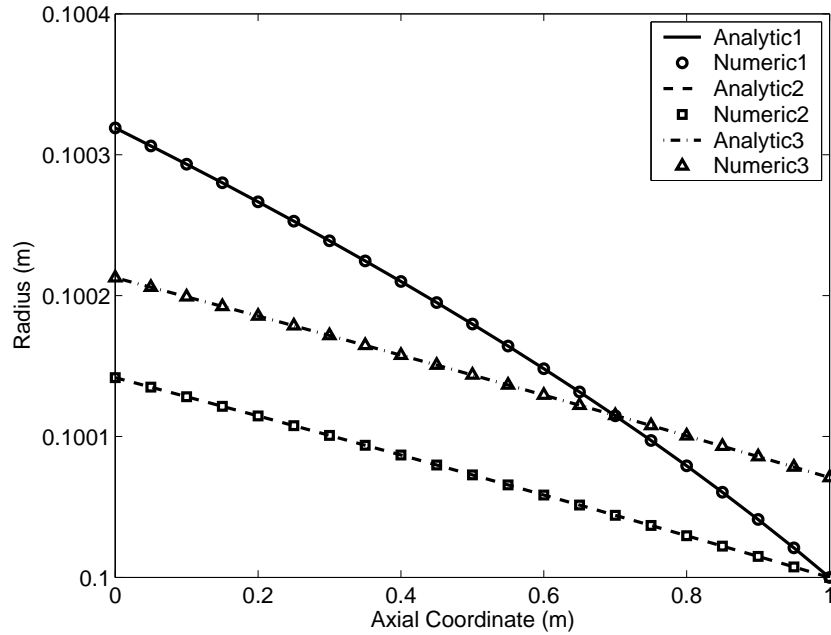

Figure 4: Radius versus tube axial coordinate for the three sample cases of Figure 3.

6 Conclusions

In this study, two analytical expressions, correlating volumetric flow rate to pressure at inlet and outlet, are derived for the Newtonian flow in cylindrical elastic tubes from a one-dimensional form of the Navier-Stokes equations. The expressions are validated numerically by a finite element method based on a Galerkin scheme with Lagrange interpolation and Gauss quadrature integration. Sample results, which are quantitatively and qualitatively sensible, are presented for demonstration. Two constitutive relations, depicting the nature of the relation between area and pressure in elastic tubes, are used in all these derivations and finite element implementation. The foundations of the finite element weak form for the two p-A models are outlined for completion. Preliminary rational trends in these results are observed and documented. Analytical implicit relations for obtaining the pressure field inside the tube, as well as the tube geometric profile, are also presented, demonstrated and numerically validated. The outcome of this investigation, numerical as well as analytical, is of relevance to several areas of science, technology and medicine.

Nomenclature

α	correction factor for axial momentum flux
β	stiffness factor in the second p-A model
γ	stiffness factor in the first p-A model
κ	viscosity friction coefficient
$\lambda_{1,2}$	eigenvalues of $\mathbf{H}$ matrix
μ	fluid dynamic viscosity
ν	fluid kinematic viscosity
ρ	fluid mass density
ς	Poisson's ratio of tube wall
$\boldsymbol{\omega}$	vector of test functions in finite element formulation
Ω	solution domain
$\partial\Omega$	boundary of solution domain
A	tube cross sectional area at pressure p
A_{in}	tube cross sectional area at inlet
A_o	tube reference cross sectional area at reference pressure
A_{ou}	tube cross sectional area at outlet
$\mathbf{B}$	matrix of force terms in the 1D Navier-Stokes equations
E	Young's modulus of tube wall
$\mathbf{F}$	flux matrix in the 1D Navier-Stokes equations
$\mathbf{H}$	matrix of partial derivatives of $\mathbf{F}$ with respect to $\mathbf{U}$
h_o	tube wall thickness at reference pressure
L	length of tube
$\boldsymbol{L}_{1,2}$	left eigenvectors of $\mathbf{H}$ matrix
p	pressure at given coordinate z
P_{in}	pressure at tube inlet
P_{ou}	pressure at tube outlet
Q	volumetric flow rate
r	radius
t	time
u	local axial speed of fluid at cross section

$\overline{u}$ mean axial speed of fluid at cross section

$\mathbf{U}$ vector of Navier-Stokes dependent variables

z tube axial coordinate

References

[1] A.H.P. Skelland. *Non-Newtonian Flow and Heat Transfer*. John Wiley and Sons Inc., 1967. 1

[2] R.B. Bird; R.C. Armstrong; O. Hassager. *Dynamics of Polymeric Liquids*, volume 1. John Wily & Sons, second edition, 1987. 1

[3] P.J. Carreau; D. De Kee; R.P. Chhabra. *Rheology of Polymeric Systems*. Hanser Publishers, 1997. 1

[4] T. Sochi. *Pore-Scale Modeling of Non-Newtonian Flow in Porous Media*. PhD thesis, Imperial College London, 2007. 1

[5] T. Sochi; M.J. Blunt. Pore-scale network modeling of Ellis and Herschel-Bulkley fluids. *Journal of Petroleum Science and Engineering*, 60(2):105–124, 2008. 1

[6] T. Sochi. Pore-scale modeling of viscoelastic flow in porous media using a Bautista-Manero fluid. *International Journal of Heat and Fluid Flow*, 30(6):1202–1217, 2009. 1

[7] T. Sochi. The flow of power-law fluids in axisymmetric corrugated tubes. *Journal of Petroleum Science and Engineering*, 78(3-4):582–585, 2011. 1

[8] T. Sochi. Newtonian Flow in Converging-Diverging Capillaries. *International Journal of Modeling, Simulation, and Scientific Computing*, 04(03):1350011, 2013. 1

[9] L. Formaggia; D. Lamponi; A. Quarteroni. One-dimensional models for blood flow in arteries. *Journal of Engineering Mathematics*, 47(3/4):251–276, 2003. 1, 2, 7

[10] S.J. Sherwin; V. Franke; J. Peiró; K. Parker. One-dimensional modelling of a vascular network in space-time variables. *Journal of Engineering Mathematics*, 47(3-4):217–250, 2003. 1, 2, 7

[11] W. Ruan; M.E. Clark; M. Zhao; A. Curcio. A Hyperbolic System of Equations of Blood Flow in an Arterial Network. *SIAM Journal on Applied Mathematics*, 64(2):637–667, 2003. 2

[12] T. Sochi. One-Dimensional Navier-Stokes Finite Element Flow Model. *Technical Report*, 2013. arXiv:1304.2320. 2, 7

[13] T. Sochi. Slip at Fluid-Solid Interface. *Polymer Reviews*, 51(4):309–340, 2011. 2

[14] S.J. Sherwin; L. Formaggia; J. Peiró; V. Franke. Computational modelling of 1D blood flow with variable mechanical properties and its application to the simulation of wave propagation in the human arterial system. *International Journal for Numerical Methods in Fluids*, 43(6-7):673–700, 2003. 7

[15] S. Čanić; E.H. Kim. Mathematical analysis of the quasilinear effects in a hyperbolic model blood flow through compliant axi-symmetric vessels. *Mathematical Methods in the Applied Sciences*, 26(14):1161–1186, 2003. 7

[16] G. Pontrelli; E. Rossoni. Numerical modelling of the pressure wave propagation in the arterial flow. *International Journal for Numerical Methods in Fluids*, 43(6-7):651–671, 2003. 7

[17] L. Formaggia; D. Lamponi; M. Tuveri; A. Veneziani. Numerical modeling of 1D arterial networks coupled with a lumped parameters description of the heart. *Computer Methods in Biomechanics and Biomedical Engineering*, 9(5):273–288, 2006. 7